A Dislocation Density Based Constitutive Model for as-cast Al-Si Alloys; Effect of Temperature and Microstructure

Mohammadreza Zamani [a]*, Hoda Dini [a], Ales Svoboda [b], Lars-Erik Lindgren [b], Salem Seifeddine [a], Nils-Eric Andersson [a], Anders E.W Jarfors [a]

[a] Department of Materials and Manufacturing, School of Engineering, Jönköping University, 551 11, Jönköping, Sweden
[b] Division of Mechanics of Solid Materials, Luleå University of Technology, 971 87 Luleå, Sweden

* E-mail: mohammadreza.zamani@ju.se

1. Abstract

The flow stress of an as-cast Al-Si based alloy was modeled using a dislocation density based model. The developed dislocation density-based constitutive model describes the flow curve of the alloy with various microstructures at quite wide temperature range. Experimental data in the form of stress-strain curves for different strain rates ranging from 10^{-4} to 10^{-1} s^{-1} and temperatures ranging from ambient temperature up to 400 ^{o}C were used for model calibration. In order to model precisely the hardening and recovery process at elevated temperature, the interaction between vacancies and dissolved Si was included. The calibrated temperature dependent parameters for different microstructure were correlated to the metallurgical event of the material and validated. For the first time, a dislocation density based model was successfully developed for Al-Si cast alloys. The findings of this work expanded the knowledge on short strain tensile deformation behaviour of these type of alloys at different temperature, which is a critical element for conducting a reliable microstructural FE-simulation.

Keywords: Aluminium cast alloy, dislocation density, vacancy concentration, Si solute, eutectic phase, Si precipitates

2. Introduction

Aluminium cast alloys have become competitive in engineering applications thanks to their light weight, high specific strength and inexpensive manufacturing process [1]. Among the aluminium cast alloys, Al-Si based alloys are the most commonly used in different industries such as automotive due to excellent castability, high wear resistance and useful mechanical properties at ambient and elevated temperature [2]. Addition of alloying elements such as Cu and Mg enhance the strength of the alloys and makes them responsive to heat treatment [3]. Although the mechanical properties of Al-Si-Cu-Mg casting alloys have been widely investigated at room temperature, their high temperature behaviour in the as-cast condition is less well studied. It is well-known that the deformation behaviour of these alloys at ambient temperature is mainly governed by microstructural features such as secondary dendrite arm spacing (SDAS) [4], size and morphology of secondary particles (e.g. eutectic Si, Al_2Cu, Mg_2Si) [5]. These obstacles to dislocation motion are randomly distributed in grain boundaries, dendrites and the eutectic regions [6]. The contribution of the strengthening elements may also change at higher temperatures where dynamic recovery takes place [7].

The active mechanisms and underlying physics, governing plastic deformation, depend on the crystallography and microstructure of the alloy as well as strain rate and temperature. Understanding of the influence of these factors is essential to develop a dislocation density-based constitutive relation expected to be able to re-produce, in a robust manner, flow stress outside the test range [8]. Several mechanisms such as dislocation glide and dislocation climb have been found to be active during plastic deformation at different operating temperatures [9]. It was reported that at a given temperature, stress and grain size are rate controlling factors [10]. In Al-Si alloys, at temperatures below half of the absolute melting temperature (T_m), dislocations pass the obstacles through thermally-activated glide. Therefore, it is regarded as the active deformation mechanism at temperatures below $0.5T_m$ irrespective of strain rate and size of

the grains [10, 11]. The same mechanism also drives plastic deformation at higher temperature and higher stress, $\sigma/G=1\times10^{-3}$ - 5×10^{-3}, where G is the temperature compensated shear modulus [10, 12]. However, at temperatures above $0.5T_m$ and σ/G values lower than 1×10^{-4}, the principal deformation mechanism is dislocation climb, which is a diffusion-controlled process.

There is a need for a reliable material model that can predict the mechanical behavior at different temperatures and deformation rates. The model would be useful in simulations to verify component performance and to reduce trial and error experimental activities. During recent decades, various empirical models have been proposed to describe the inelastic behavior of FCC materials [13, 14] and in particular Al alloys [15, 16]. The most well-known are power-law models [13, 14] where plastic strain varies as a power of applied stress. These empirical models are primarily derived from curve-fitting and their validity at different temperatures and strain rates is quite limited. Although there are some hardening models that can be obtained from empirical models and models based on dislocation mechanisms (e.g. power law creep [17]), not considering the underlying physical process restricts their range of validity [8, 18]. In the models based on physics of material, the underlying physical process, dislocation processes etc. are used to formulate the constitutive equations [8]. Dislocation density is the microstructural variable that governs the properties [19], and leads to an understanding about physics of the material [8]. A change in density of mobile dislocation is related to the slip system and as well as thermally activated annihilation by dislocation climb. The immobilization rate of mobile dislocations is a function of microstructure, strain rate and temperature. The recovery process occurs through climb [19] and glide of dislocations [20]. The diffusion of vacancies, which usually takes place at elevated temperature, is a dominant factor in the recovery process. The high concentration of vacancies near grain boundaries enhances creep controlled by dislocation glide and climb processes [21]. Lindgren et al. [8] proposed a dislocation density model in order to describe the plasticity of an austenitic stainless steel. This model was subsequently employed by others in order to describe plastic deformation and flow stress behavior of Ti-6Al-4V [22] and Al-5Mg (AA5083) alloy [23] at different temperatures. The model was primarily developed as a reliable input for FE simulation of thermo-mechanical manufacturing processes (forming, welding, splaying) where the empirical models are not expected to yield the desired results as well as "large scale computations" where discrete dislocation models can not be used. Different approaches were employed by researchers in order to formulate a physically based model for metal plasticity. Since the discrete dislocation modelling approach is computationally expensive for the simulation of manufacturing process, average dislocation density model is used in this study [24, 25]. This model considers the alloy as a single phase material containing particles, and describes hardening/softening behaviour based on dislocation density and excess vacancies. Subsequently, the predicted behaviour could be utilized in casting simulation software for the final design in order to obtain desired mechanical material behaviour on a local level in the cast components [26, 27]. To the authors' knowledge there is no prior work on modelling capable to describe the temperature dependent deformation behaviour of Al-Si-Cu-Mg cast alloys. It is therefore a useful exercise to develop a dislocation density-based model able to predict their flow stress.

In the present paper, a dislocation-based model derived from tensile test data was developed and employed to describe and predict the flow stress of the EN AC-46000 aluminum casting alloy at small strain regime for various microstructures from ambient temperature to 400 ºC and strain rates from 10^{-4} to 10^{-1} s^{-1}. The effects of temperature and microstructural features on temperature-dependent parameters of the model are discussed and linked to the underlying metallurgical event which control the deformation behavior in this type of materials.

3. Experimental

3.1 Material

The alloy used in this study was EN AC-46000, containing (in wt. %) 10.0 Si, 2.6 Cu, 0.24 Mg, 0.8 Fe, 0.8 Zn and 0.26 Mn, balance Al. The alloy was cast at 730 °C to ensure mould filling. To vary the microstructure, a second melt was prepared with addition of 0.04 wt.% Sr, using Al-10%Sr master alloy. The alloy was gravity die cast into rods (length 20 cm, diameter 1 cm) in a copper mould. Since presence of casting defects encourage premature failure under static and dynamic load [28], a directional solidification set-up was employed to minimize these uncertainties and obtain a homogeneous and isotropic casting. Therefore, the cast rods were re-heated to 710 °C, which is sufficient temperature for re-melting, and held for 20 minutes under Ar-atmosphere in a Bridgeman furnace. The furnace was raised at the prescribed speed while the sample remained in a stationary position. The microstructural length-scale, i.e. the secondary dendrite arm spacing, was controlled by varying the furnace raising speed. To achieve microstructures with similar length scales to those obtained by high pressure die casting (HPDC) and gravity die casting, raising speed were set to 3 and 0.3 mm s^{-1}, which lead to SDAS of 10 and 25 μm respectively [29]. In Bridgman furnace processed samples, the major part of the sample length solidifies under steady state producing homogenous microstructure. Samples for tensile testing and material characterization were taken from the steady state section.

3.2 Tensile Testing

Cylindrical tensile test bars according to ASTM B557M-10 [30], 6 mm in diameter and 100 mm in length were prepared from the as-cast rods by machining. Tensile tests were carried out using a Zwick/Roell Z100 testing machine, at five different temperatures ranging from of 25 ºC to 400 ºC. Strain rates used ranged from 10^{-4} to 10^{-1} s^{-1}. Prior to tensile testing, the specimens were heated to the test temperature and held for 15 minutes to homogenise the specimen temperature. At least four samples were tested for each condition.

3.3 Characterization of the microstructure

The microstructure was studied by optical microscopy, (OLYMPUS GX71). The concentration of the Si solutes in the dendrites was measured by scanning electron microscopy (JEOL7001F) equipped with Wavelength-Dispersive X-ray Spectroscopy (WDS). Since WDS analysis offers higher peak to background ratio rather than EDS analysis, it was employed to measure the solute concentration in the dendrites. A longitudinal area of 10×30 mm^2 from the centre of directionally solidified specimens characterized through EBSD and optical microscopy (EDAX, Digiview 3 camera) using JEOL 7001F scanning electron microscope at an accelerating voltage of 25 kV with 5 μm step size. A multifield EBSD data collection was done to cover a relatively large area for grain size measurement. Differential scanning calorimeter (DSC) analyses were carried out to detect non-equilibrium reactions that may occur during heating. DSC was performed under purified argon atmosphere using a NETZSCH 404C Pegasus® instrument at a scan rate of 5°C/min in the temperature range 27 - 400 ºC.

4. The flow stress model

According to the work by Bergström [31] and Kocks [32], the flow stress is assumed to consist of two major components, (equation 1):

$$\sigma_y = \sigma^* + \sigma_G \quad (1)$$

where σ^* is the thermally activated stress needed to overcome short range barriers and σ_G is the athermal stress contribution from the long-range interactions of the dislocation substructure. The short-range stress component is written as [9, 32, 33];

$$\sigma^* = \tau_0 G\left\{1-\left[\frac{kT}{\Delta f_0 G b^3}\ln\left(\frac{\dot{\bar{\varepsilon}}^{ref}}{\dot{\bar{\varepsilon}}^{pl}}\right)\right]^{1/q}\right\}^{1/p} \qquad (2)$$

where τ_0 is a dimensionless optimisation factor, G is shear modulus, $\tau_0 G$ is the athermal flow strength required to move the dislocation passed the barriers (precipitates and particles) without aid of thermal energy, k is the Boltzmann constant, T is the temperature, Δf_0 is dimensionless optimisation factor, $\Delta f_0 G b^3$ is the required activation energy to overcome lattice resistance in the absence of external forces [34], b is the Burgers vector, $\dot{\bar{\varepsilon}}^{ref}$ is a constant to a first approximation and is called the reference strain rate [35] and $\dot{\bar{\varepsilon}}^{p}$ is the applied strain rate. The exponents p and q characterise the shape of the energy barriers and have the values of $0 < p \leq 1$ and $0 < q \leq 2$ [9, 32, 33].

The long-range barriers are due to interactions with the dislocation substructure and are related to the immobile dislocation density, written as equation (3) [36]:

$$\sigma_G = m\alpha G b\sqrt{\rho_i} \qquad (3)$$

where *m* is the Taylor orientation factor, α is a proportionality parameter, ρ_i is the immobile dislocation density and *G* is a temperature dependent shear modulus (computed from the elastic modulus, E, and the Poisson ratio *v*). The mobile dislocation density is assumed to be much smaller than the immobile density according to Bergström [37] and Estrin [38]. In the model, the density of immobile dislocations ρ_i consists of hardening (+) and recovery (-) terms. Mobile dislocations are included through the hardening and annihilation processes as they move the length of the average of mean free path (Λ), before they are immobilized or annihilated during hardening process, see equation 4. According to the Orowan equation, density of mobile dislocations and their average velocity are proportional to the plastic strain rate. As long as the strain rate is quite small the temperature may not increase the density of mobile dislocation. This was also assumption in the other works by Bergström [39] and Estrin [38].

$$\dot{\rho}_i^{(+)} = \frac{m}{b}\frac{1}{\Lambda}\dot{\bar{\varepsilon}}^{p} \qquad (4)$$

The mean free path (Λ) is generally assumed to be a combination of the grain size, g, Secondary Dendrite Arm Spacing SDAS, dislocation subcell size, s, and microstructural constituents as formulated in equation (5):

$$\frac{1}{\Lambda} = \frac{1}{g} + \frac{1}{\mathrm{SDAS}} + \frac{1}{s} + \ldots \qquad (5)$$

In Al-Si cast material the yield point is primarily governed by SDAS rather than grain structure, at larger strain, the mean free path will be influenced strongly by dislocation subcell size [5, 29, 40]. The density of immobile dislocations is reduced during recovery process due to glide and climb. The term which is controlled by glide is proportional to the current dislocation density and the plastic strain rate, and is formulated as equation (6) [39]:

$$\dot{\rho}_{i\,(glide)}^{(-)} = \Omega\rho_i\dot{\bar{\varepsilon}}^{p} \qquad (6)$$

where Ω is a dimensionless optimisation recovery function that depends on temperature in the current model. This equation takes only dynamic recovery into the consideration due to the strain rate. Although the recovery function is

denoted in term of recovery by climb, it may include recovery by glide or cross-slip as the formulation is combination of the model used by Militzer et al. [41] and Siwecki & Engberg [42]. Static recovery, however, is controlled by diffusion climb having the following formulation in equation (7) [8, 41]:

$$\dot{\rho}_i^{(-)}{}_{(\text{climb})} = 2c_\gamma D_v \frac{c_v}{c_v^{eq}} \frac{Gb^3}{kT}\left(\rho_i^2 - \rho_{eq}^2\right) \qquad (7)$$

where c_v^{eq} and c_v are the equilibrium and current vacancy concentration, and c_γ is a calibration parameter. In FCC metals, the strain-induced vacancy concentration is significant due to their low diffusivities. A model for excess vacancy concentration with generation and annihilation components has been proposed by Militzer *et al* [41]. In the present model, it is assumed that only long-range stress contributes to vacancy formation and only mono-vacancies are concerned. When a crystal is held for a sufficient time at a given temperature, an equilibrium level of vacancies is reached. Deforming the material or changing the temperature generally generates excess vacancies. The effect of excess vacancies on diffusion is taken into account as the equation (8).

$$\dot{c}_v^{ex} = \dot{c}_v - \dot{c}_v^{eq} = \left(\chi \frac{\sigma_y b}{Q_{vf}} + \varsigma \frac{c_j}{4b^2}\right)\frac{\Omega_0}{b}\dot{\bar{\varepsilon}}^p - D_{vm}\left(\frac{1}{s^2} + \frac{1}{\lambda^2}\right)\left(c_v - c_v^{eq}\right) \qquad (8)$$

where the factor χ is the fraction of the mechanical work needed for the vacancy formation, Q_{vf} is the activation energy for forming a vacancy, Ω_0 is the atomic volume and c_j is the concentration of thermal jogs. The parameter ς describes the neutralisation effect by vacancy emitting and absorbing jogs, c_v^{eq} is the equilibrium concentration of vacancies at a given temperature, c_v is the non-equilibrium vacancy concentration, D_{vm} is the vacancy migration and stress σ_y is the flow stress. Details of the model and stress update algorithm are found in Lindgren *et al.* [8].

In order to develop the model for the prediction of the deformation behaviour of these materials, a set of parameters have to be derived from the experimental flow curves as well as data related to the alloy which is extracted from the literature and summarised in Table 1. The constants were chosen either for Al-Si alloy or for pure Al based on availability in the literatures. The Taylor factor (m) is corresponding for Al alloy including the effect of addition of alloying elements [9, 43]. Self-diffusion activation energy (Q_v) for Al-Si interdiffusion is equal to 148.6 kJmol^{-1} [35, 44, 45], while the self-diffusion activation energy for pure Al = 140 kJmol^{-1} [35], in current model the value close to the average was considered. The value for initial vacancy diffusivity (D_{vm}) corresponds to pure Al [35], however the values reported for Al alloys are in the same range [44, 46]. The constant for the entropy of vacancy formation (ΔS_{vf}) corresponds to cubic metals [47].

Table 1. The constants which were used in the model.

Parameter	Notation	Value	Dimension	References & Comments
Boltzmann's constant	k	1.38×10^{-23}	JK^{-1}	[41]
Burger's vector	b	2.86×10^{-10}	m	[23, 48]
Melting temperature	T	660	°C	[49]
Taylor factor	m	3.06	-	[9, 43]
Atomic volume	Ω_0	1.66×10^{-29}	m^3	[35]
Young's modulus at room temperature	E	65	GPa	Evaluated from tensile test at room temperature

Shear modulus	G	24.4	GPa	Calculated
Poisson's ratio	υ	0.33	-	[50]
Self-diffusion activation energy	Q_v	140	$kJmol^{-1}$	[35, 44, 45]
Activation energy of vacancy formation	Q_{vf}	74.3	$kJmol^{-1}$	[45, 51]
Energy barrier for vacancy migration	Q_{vm}	65.7	$kJmol^{-1}$	$Q_v = Q_{vf} + Q_{vm}$
Initial vacancy diffusivity	D_{vm}	1.71×10^{-4}	m^2s^{-1}	[35]
Pipe diffusivity	D_{p0}	4.0×10^{-5}	m^2s^{-1}	[35]
Reference strain rate	$\dot{\bar{\varepsilon}}_{ref}$	10^6	s^{-1}	[52]
Increased entropy upon creating a vacancy	ΔS_{vf}	1.92×10^{3}	JK^{-1}	[47]
Fraction of mechanical work for vacancy formation	χ	0.1	-	[41]
Formation energy of thermal jogs	Q_{fi}	3.53×10^{-20}	J	[41]
Neutralisation effect by vacancy emitting and absorbing jogs	ς	10	-	[41]
Initial immobile dislocation density	ρ_{i0}	10^{12}	m^{-2}	[52]

5. Calibration and validation of the model

5.1 The addition of Si-vacancy interaction

Addition of Si to Al decreases the vacancy formation energy [53] and increases the concentration of vacancies particularly near the Si solute atoms [54]. The generation, motion and interaction of vacancies are coupled with the diffusion of solute atoms and hence dislocation recovery. The current model considers the material as a mono-phase matrix containing reinforcing particles (e.g. precipitates and secondary phases). The role of the Si solute during hardening has been considered through equation (2) as the parameter Δf_0. However the interaction with vacancies, their effect on excess vacancy formation and on vacancy annihilation processes has not been considered in the initial model. Therefore, a correction term was added to provide a better description of the recovery process assisted by vacancy formation. Using the relation proposed by Lomer [54], the interaction between Si solute atoms and vacancies can be estimated (equation 9):

$$\frac{X_{vac}^{Al-Si}}{X_{vac}^{Al}} = 1 - \mathrm{Z}\mathrm{X}_{\mathrm{Si}} + ZX_{Si}\exp\left(\frac{E}{kT}\right) \qquad (9)$$

where Z is the coordination number, X_{si} is concentration of solute, E (J) is the vacancy-Si binary interaction energy in Al, and k (JK^{-1}) is Boltzmann's constant. The concentration of solute in the matrix (X_{si}) was measured using WDS technique. X_{si} (the value for SDAS 10 and 25 μm) was then given as 0.014 and 0.015 respectively, Z was set to 12 (for FCC materials [54]) and E was set to 1.6×10^{-19} [55]. The value of c_υ^{eq} which is the corresponding value for Al in equation (7) is then multiplied by the correction scale, equation 8. Figure 1 shows the influence of the correction scale addition on the predicted flow curve.

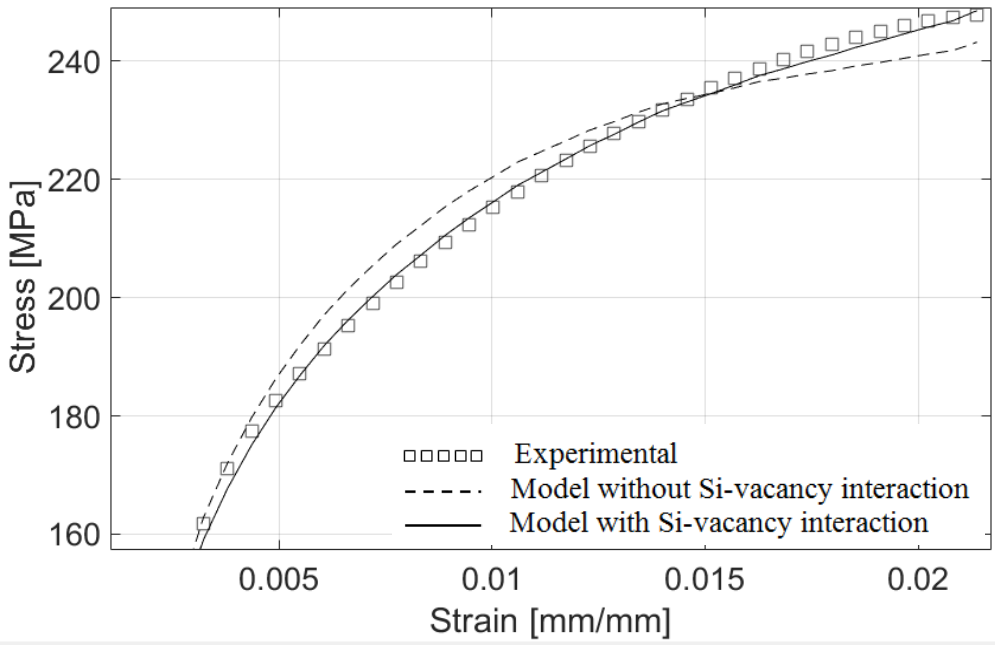

Figure 1. The calculated flow curve with and without the correction factor. SDAS 10 µm at 200 ºC. Strain rate is equal to 10^{-4} s^{-1}.

The value of the correction varies from 10^{7} to 10^{16}, which means a significant increase in the equilibrium vacancy concentration. The correction resulted in a more precise description of the flow curves under all conditions; however, the level of improvement in fitting was different from case to case.

5.2 Validation of the manufacturing technique

In order to investigate the role of microstructure on the calibrated parameters of the model, diversified microstructure was generated.

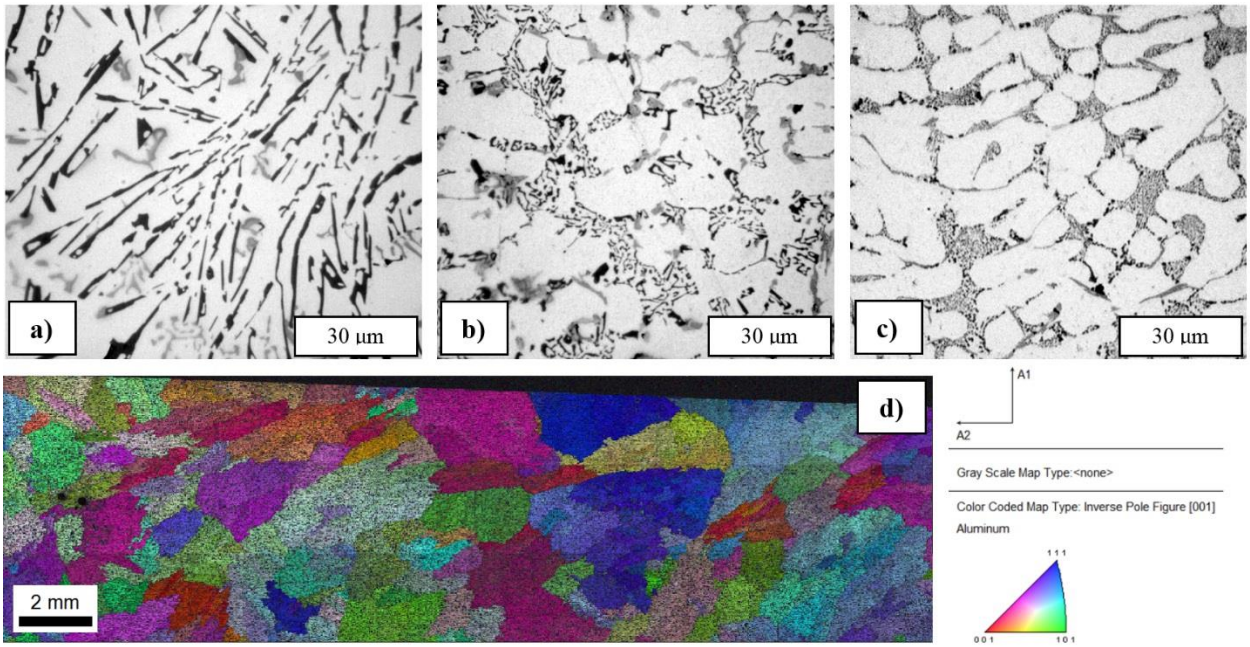

Figure 2(a), (b) and (c) show the microstructural features of the alloy with SDAS 25 µm as well as SDAS 10 µm (in unmodified and modified conditions). The SDAS was measured from groups of well-defined secondary arms. The

manufactured samples (directionally solidified) needed to act as a continuum and display isotropic behavior. The Figure 2(c) shows a false colour reconstruction of grains in a 10 µm SDAS Sr-modified sample using EBSD orientation mapping. The map shows adequate random crystallite orientation suggesting that there is no texture anisotropy in the samples. Furthermore, although the samples comprise relatively large grains (~ 1-2 mm), an adequate number of grains was obtained in the samples considering the misorientation angle of 15º as the boundary limit. The grain size and average SDAS for different conditions are summarized in Table 2.

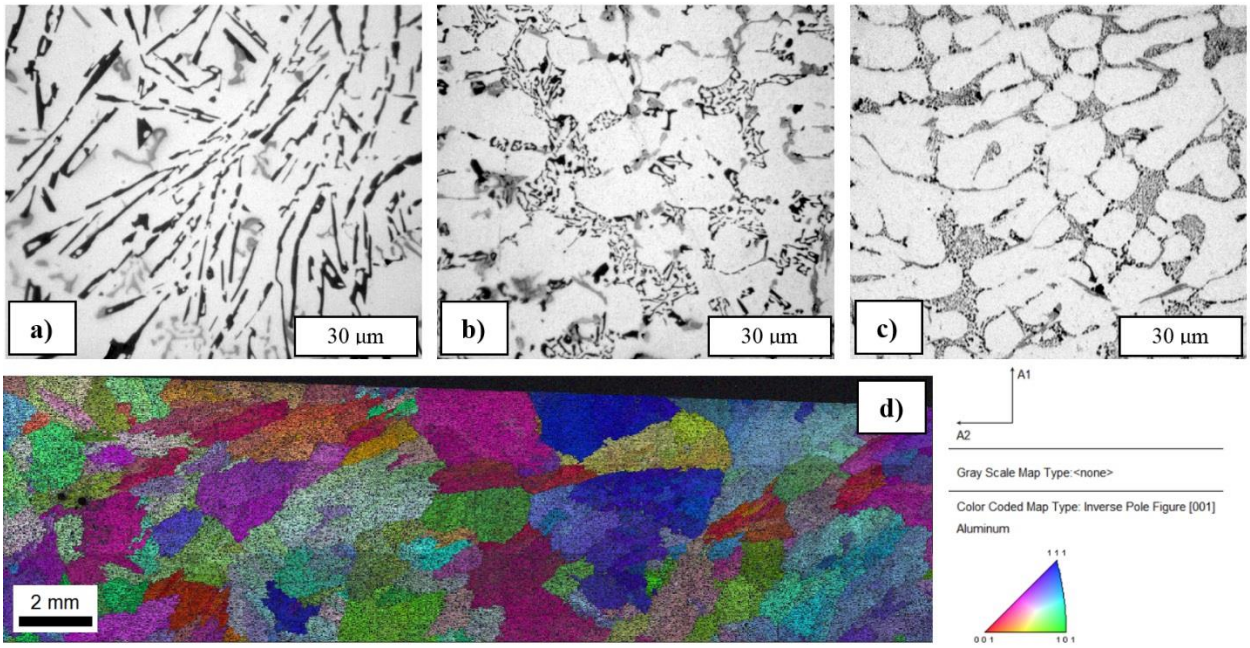

Figure 2 The micrographs illustrate the microstructure corresponding to a**)** Unmodified SDAS 25 µm, b**)** Unmodified SDAS 10 µm, c) Modified SDAS 10 µm and, d) reconstructed EBSD map of the modified alloy with SDAS 10 µm .

Table 2 SDAS and grain size of different as-cast microstructures.

Furnace pulling rate (mm/s)	Sr level (wt.%)	SDAS (µm)	Grain size (mm)
0.3	-	25.9 ± 3.5	2.10 ± 0.36
3	-	10.1 ± 2.3	1.19 ± 0.28
3	0.04	10.4 ± 2.1	1.32 ± 0.30

5.3 Calibration of stress–strain curves

The tensile test results for the materials tested in various conditions are presented in Figure 3 and Figure 4. The role of microstructural coarseness (SDAS), strain rate and testing temperatures are clearly demonstrated. Typical experimental and predicted flow stress curves, are plotted in Figure 3 and 4. Curves corresponding to different coarseness of microstructure (SDAS 10 and 25 µm) and the Sr-modified microstructure at different temperature are plotted in Figure 3. The influence of strain rate can be observed in the series of curves in Figure 4.

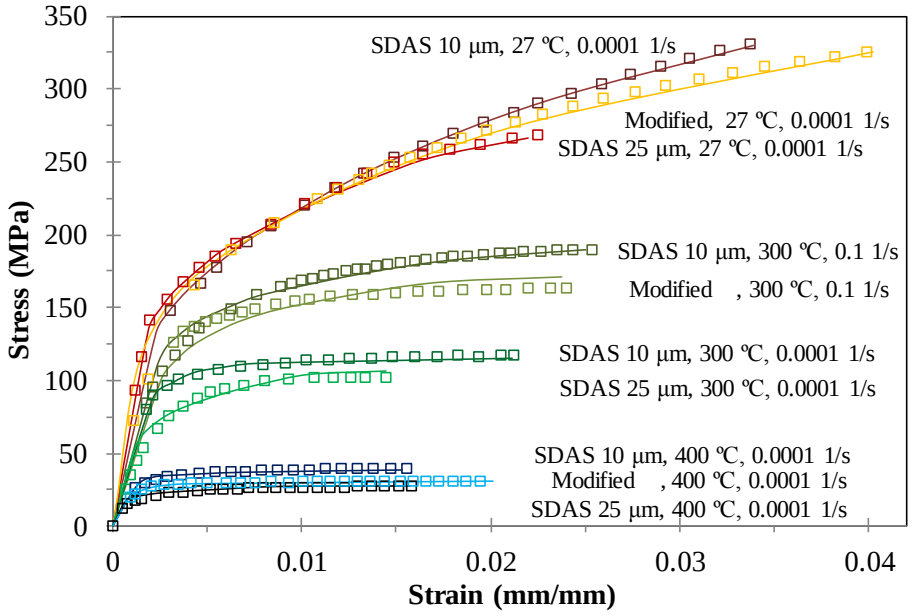

Figure 3 Measured and calculated true stress – true strain curves for unmodified (SDAS 10 µm and 25 µm) and modified alloys from ambient temperature to 400 ºC. Calculated = solid lines.

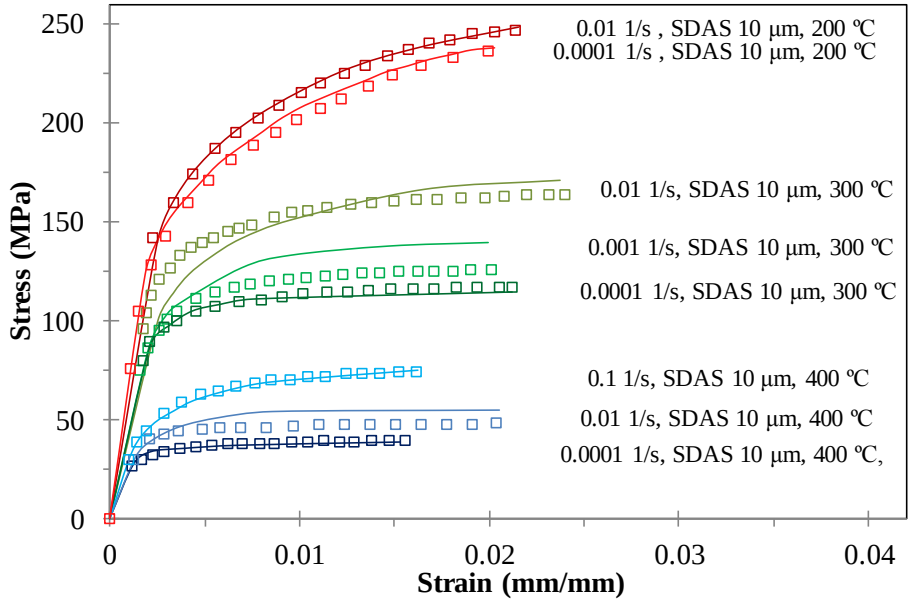

Figure 4 Measured and calculated true stress – true strain curves for SDAS 10 µm at strain rates of 10^{-4} to 10^{-1} from 200 to 400 ºC. Calculated = solid lines.

The measured values have been smoothed in order to remove serrations due to measurement noise. Residual mean square (RMS) of smoothed curve and experimental results for the case having the largest serrations was calculated to be 0.31 MPa (calculated for 20 points). The hollow squares show the experimental data, while the solid lines indicate the calculations using the material model. The overall match is reasonable between the experimental and computed flow stress curves for any given test conditions, see Figure 3. This is primarily due to the addition of a correction term which includes the effect of solute concentration in the α-Al, see equation (8). This as a result influences the initial hardening stage ($\varepsilon < 0.02$) and consequently alters the shape of the flow stress curves [56]. However, there is still some deviation between the measured and calculated data, particularly for the case of SDAS 10 µm at 300 ºC. This

may be due to experimental errors in the furnace temperature. RMS of model and experimental curve for the case showed the highest deviation, was calculated to be 3.3 MPa (calculated for 20 points) while most of the cases obtained RMS smaller than 0.1 suggesting quite high fitting accuracy. In the range of 200-300 ºC Si precipitation takes place which change the curves format where the slight miss-fitting were seen, Figure 4. It should be noted that although the test samples experienced quite large strain deformation, especially above 300 ºC, the model used the experimental data obtained before tensile instability occurred. Tensile instability is the point that necking or localized deformation commence. In this event, increase in stress due to decrease in the cross-sectional area of the specimen become greater than the increase in the load carrying ability of the alloy due to strain hardening. The strain that necking occurred is realized through meeting the true stress-true strain curve with its derivative according to the criterion of $\sigma = d\sigma/d\varepsilon$ [50]. The parameters from the model which are temperature and microstructure dependant are listed in Table 3.

Table 3 Calibrated parameters as a function of temperature for different as-cast conditions.

Parameters	T (ºC)	27	100	200	300	400
τ_0	SDAS 10 μm - Modified	0.0078	0.0079	0.0114	0.0144	0.0140
	SDAS 10 μm - Unmodified	0.0072	0.0086	0.0127	0.0128	0.0127
	SDAS 25 μm - Unmodified	0.0085	0.0090	0.0118	0.0138	0.0118
Δf_0	SDAS 10 μm - Modified	0.839	0.859	1.184	1.077	0.855
	SDAS 10 μm - Unmodified	0.856	1.031	1.258	1.279	1.077
	SDAS 25 μm - Unmodified	0.957	0.923	1.078	1.094	1.099
Ω	SDAS 10 μm - Modified	44.3	60.1	79.7	144.0	259.0
	SDAS 10 μm - Unmodified	45.9	75.1	119.1	146.7	256.2
	SDAS 25 μm - Unmodified	48.5	62.9	115.0	146.6	249.1
K_c	Modified: 25	SDAS 10 μm : 29		SDAS 25 μm : 23		
c_γ	Modified: 0.31	SDAS 10 μm : 0.63		SDAS 25 μm : 0.05		
p	Modified: 1.00	SDAS 10 μm : 0.64		SDAS 25 μm : 0.55		
q	Modified: 2.00	SDAS 10 μm : 1.43		SDAS 25 μm : 1.46		
α	1.42					

5.4 Validation of temperature dependent variables of the model

The present model assumes the material is a single-phase deforming matrix containing reinforcing particles. Three temperature dependent parameters (τ_0, Δf_0 and Ω) have key role in describing the hardening and recovery during deformation. These fit parameters are unique solutions of the calibration and describe proper type of physic / metallurgical phenomena in the material. A physical relevance between fit parameters and hardening process / dislocation annihilation was found and elaborated in what follows. The parameter τ_0 controls the quality and magnitude of the effect of reinforcing particles during the hardening process. The quantity $\tau_0 G$ in equation (2) is athermal stress related to the strength of precipitates in the matrix. The values of τ_0 are relatively low (<0.013) compared to the values for Al5Mg wrought alloy (0.013-0.06) [23] and Ti6Al4V (0.1 - 3.5) [57]. This suggests that the precipitate contribution to the yield strength is low at all temperatures. Figure 5 shows the quantity of τ_0 as a function of temperature for both SDAS 10 and 25 μm (solid lines). The magnitude of τ_0 was small for both unmodified and Sr-modified structure supporting that it is possible to model the material as a single phase materials with particles instead of a dispersion hardened material or composite. Furthermore, it was seen that τ_0 value increases at temperatures above 200 ºC, which suggests that the contribution from precipitated to the yield strength increases. According to the equilibrium phase diagram, Si has a maximum solubility in Al of 1.6 wt. % at 576 ºC, which is lowered to 0.26 wt. % at 400 ºC. The WDS analysis indicated 1.45 ± 0.10 wt. % Si in the α-Al dendrites for both coarseness of microstructure. Hence, an initial composition of 1.5 wt. % supersaturated Si was assumed for the as-cast condition. Typical DSC traces obtained during heating show an exothermic peak in the temperature range of 200-300 ºC which corresponds to Si precipitation [58], see Figure 5. The kinetics of Si precipitation is closely linked to the amount of excess vacancy [59, 60]. A

considerable fraction of the vacancies form a significant number of loops which act as heterogeneous nucleation sites for precipitation of Si atoms [61, 62].

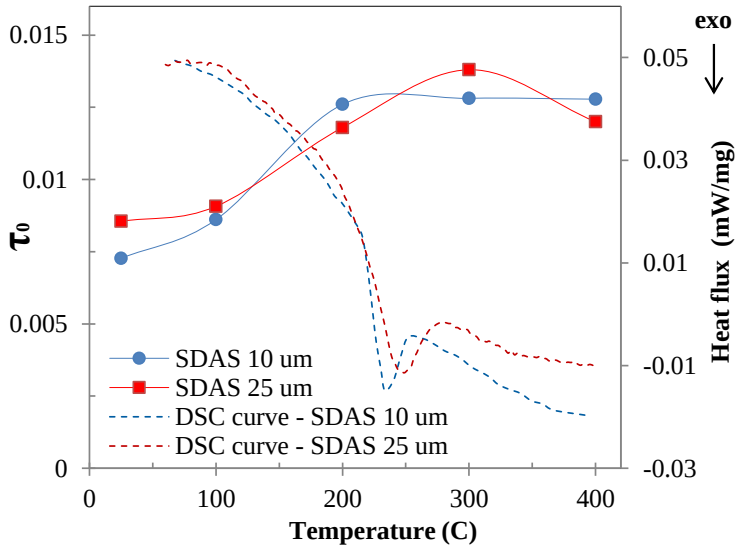

Figure 5. The τ_0 as a function of temperature, and DSC thermograms of the alloy with SDAS 10 and 25 µm.

The formation of Si precipitates explains the intensified effect of the reinforcing particle on hardening, which is reflected as the increase in the magnitude of τ_0. However, as it was mentioned earlier the values of τ_0 is quite small suggesting that the contribution of particles (e.g secondary particles and precipitates) in hardening process in low strain is negligible. Spheroidisation of Si-particles and dissolution of other phases will not occur under the current test conditions and durations, nor will recrystallisation and grain growth [63].

The quantity Δf_0 is a dimensionless scaling factor corresponding to the activation energy to overcome lattice resistance or obstacles without aid from external stress [9]. The temperature variations in Δf_0 prove that the short-range stress σ^* is influenced by temperature changes. The variation however is not significant, and the Δf_0 values for different microstructure are approximately constant.

The Ω parameter describes the recovery process induced by dislocation glide and annihilation, equation (6). The variation of Ω could be also related to cross-slip depending on the mean free path. The optimized Ω values were increased by increase in temperature, with quite similar trends for the different microstructures. The inverse dependency of Ω with temperature is plotted in Figure 6, showing an exponential relationship, $\Omega = A\exp(-Q_{\text{dislocation-glide}}/RT)$ where A is an empirical constant, R is the gas constant and $Q_{\text{dislocation-glide}}$ is the activation energy for dislocation glide. The corresponding activation energy for dislocation glide was calculated to be in the range of (6-7 kJmol^{-1}) which is quite a low value. The corresponding value found to be around 10 kJmol^{-1} for the Al5Mg alloy [23] which in the same range of as-cast Al-Si alloys in this study. Roter et al. [43] indicated that the activation energy for dislocation glide could be expected to be low as the activation energy for particle cutting which is of the order $Gb^3/4\pi$ (31 kJ/mole for this case). α which is a proportionality parameter of Taylor factor, was set constant in as much as number of active slip system does not change by temperature increase,

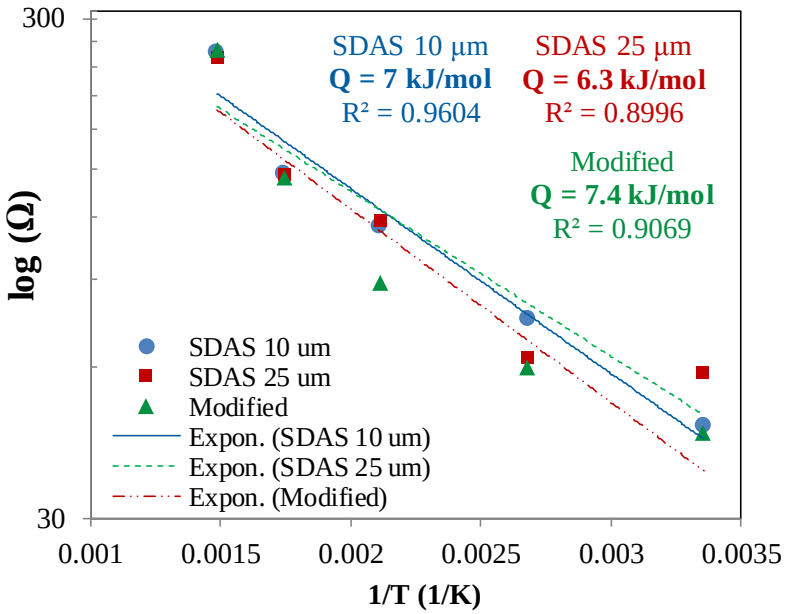

Figure 6. Ω as a function of temperature for different microstructures.

6. Conclusions

A physically-based dislocation model with the interaction between dissolved Si and vacancies was optimized to describe the as-cast flow stress behavior of EN AC-46000 casting alloy at small strain regime. The base model had been introduced for wrought materials, in this work the model was adopted and successfully improved for a cast material for the first time. The model describes the flow curves of the alloy from ambient temperature up to 400 ºC, strain rates from 10^{-4} up to 10^{-1} s^{-1} and different microstructural scale. The scaling factor, which include the role of Si solute in hardening and recovery process, improved the accuracy of the predicted flow stress curves. The contribution of particles (e.g eutectic Si, secondary particles and precipitates) in hardening of the alloy in small strain regime is negligible holding quite small τ_0 values at all temperature range. It is therefore plausible to employ the mono-phase material model for the prediction of such alloys having rather large secondary particles. The predicted behaviour is suitable input for simulation in order to obtain desired mechanical material behaviour on a local level in the cast components.

7. Acknowledgments

The author would like to acknowledge the Knowledge Foundation for supporting the CompCAST project, grant number 20100280 and Kongsberg Automotive AB and Stena Aluminum AB for support and materials as part of their undertaking in this project.

8. References

1. Handbook, A., *Properties and Selection: Non ferrous alloys and special purpose*. 1985, New York. ASM Internacional.
2. Wang, L., M. Makhlouf, and D. Apelian, *Aluminium die casting alloys: alloy composition, microstructure, and properties-performance relationships.* International Materials Reviews, 1995. **40**(6): p. 221-238.
3. Caceres, C., I. Svensson, and J. Taylor, *Strength-ductility behaviour of Al-Si-Cu-Mg casting alloys in T6 temper.* International Journal of Cast Metals Research, 2003. **15**(5): p. 531-544.
4. Caceres, C., C. Davidson, and J. Griffiths, *The deformation and fracture behaviour of an Al□ Si□ Mg casting alloy.* Materials Science and Engineering: A, 1995. **197**(2): p. 171-179.
5. Wang, Q., *Plastic deformation behavior of aluminum casting alloys A356/357.* Metallurgical and Materials Transactions A, 2004. **35**(9): p. 2707-2718.
6. Benzerga, A.A., et al., *Smaller is softer: an inverse size effect in a cast aluminum alloy.* Acta Materialia, 2001. **49**(15): p. 3071-3083.
7. Garza-Delgado, A., K. Kabiri-Bamoradian, and R.A. Miller, *Determination of Elevated-Temperature Mechanical Properties of an Aluminum A380.0 Die Casting Alloy in the As-Cast Condition.* Die Casting Engineer, 2008. **52**(6): p. 40-46.
8. Lindgren, L.-E., K. Domkin, and S. Hansson, *Dislocations, vacancies and solute diffusion in physical based plasticity model for AISI 316L.* Mechanics of Materials, 2008. **40**(11): p. 907-919.
9. Frost, H.J. and M.F. Ashby, *Deformation mechanism maps: the plasticity and creep of metals and ceramics*. 1982: Pergamon press.
10. Mahidhara, R. and A. Mukherjee, *High temperature flow and failure processes in an Al–13 wt% Si eutectic alloy.* Journal of Materials Science, 1997. **32**(3): p. 809-814.
11. Stouffer, D.C. and L.T. Dame, *Inelastic deformation of metals: models, mechanical properties, and metallurgy*. 1996: John Wiley & Sons.
12. Cahn, R.W., P. Haasen, and E.J. Kramer, *Materials Science and Technology: a Comprehensive Treatment. Vol. 8. Structure and Properties of Nonferrous Alloys.* VCH Verlagsgesellschaft mbH, P. O. Box 10 11 61, Weinheim, D-69451, Germany, 1996. 837, 1996.
13. Hollomon, J.H., *Tensile deformation.* AIME TRANS, 1945. **12**(4): p. 1-22.
14. Ludwigson, D., *Modified stress-strain relation for FCC metals and alloys.* Metallurgical Transactions, 1971. **2**(10): p. 2825-2828.
15. Alankar, A. and M.A. Wells, *Constitutive behavior of as-cast aluminum alloys AA3104, AA5182 and AA6111 at below solidus temperatures.* Materials Science and Engineering: A, 2010. **527**(29): p. 7812-7820.
16. Gelin, J., O. Ghouati, and R. Shahani, *Modelling the plane strain compression test to obtain constitutive equations of aluminium alloys.* International journal of mechanical sciences, 1994. **36**(9): p. 773-796.
17. Nabarro, F., *Thermal activation and Andrade creep.* Philosophical magazine letters, 1997. **75**(4): p. 227-233.
18. Lee, W. and X. Wen, *A dislocation-based model of forming limit prediction in the biaxial stretching of sheet metals.* International journal of mechanical sciences, 2006. **48**(2): p. 134-144.

19. Ma, A. and F. Roters, *A constitutive model for fcc single crystals based on dislocation densities and its application to uniaxial compression of aluminium single crystals.* Acta materialia, 2004. **52**(12): p. 3603-3612.
20. Blum, W., P. Eisenlohr, and F. Breutinger, *Understanding creep—a review.* Metallurgical and Materials Transactions A, 2002. **33**(2): p. 291-303.
21. Bae, D. and A. Ghosh, *Grain size and temperature dependence of superplastic deformation in an Al–Mg alloy under isostructural condition.* Acta materialia, 2000. **48**(6): p. 1207-1224.
22. Babu, B., *Physically based model for plasticity and creep of Ti-6Al-4V*. 2008: Division of Material Mechanics, Luleå University of Technology.
23. Liu, J., et al., *Finite element modelling of superplastic-like forming using a dislocation density-based model for AA5083.* Modelling and Simulation in Materials Science and Engineering, 2013. **21**(2): p. 025006.
24. Roberts, W. and Y. Bergström, *The stress-strain behaviour of single crystals and polycrystals of face-centered cubic metals—a new dislocation treatment.* Acta Metallurgica, 1973. **21**(4): p. 457-469.
25. Mecking, H. and Y. Estrin, *The effect of vacancy generation on plastic deformation.* Scripta Metallurgica, 1980. **14**(7): p. 815-819.
26. Olofsson, J. and I.L. Svensson, *Incorporating predicted local mechanical behaviour of cast components into finite element simulations.* Materials & Design, 2012. **34**: p. 494-500.
27. Olofsson, J. and I.L. Svensson, *The effects of local variations in mechanical behaviour – Numerical investigation of a ductile iron component.* Materials & Design, 2013. **43**: p. 264-271.
28. Miyazaki, T., et al., *Prediction of high-cycle fatigue life reliability of aluminum cast alloy from statistical characteristics of defects at meso-scale.* International Journal of Mechanical Sciences, 2008. **50**(2): p. 152-162.
29. Olofsson, J., et al., *Characterisation and investigation of local variations in mechanical behaviour in cast aluminium using gradient solidification, Digital Image Correlation and finite element simulation.* Materials & Design, 2014. **56**: p. 755-762.
30. *Standard Methods of Tension Testing Wrought and Cast Aluminum and Magnesium Alloy Products. ASTM B557M-10.* Annual Book of ASTM Standards. American Society for testing and Materials 2010.
31. Bergstrom, Y., *Dislocation model for the stress-strain behaviour of polycrystalline alpha-iron with special emphasis on the variation of the densities of mobile and immobile dislocations.* MAT SCI ENG, 1970. **5**(4): p. 193-200.
32. Kocks, U., *Laws for work-hardening and low-temperature creep.* Journal of Engineering Materials and Technology, 1976. **98**(1): p. 76-85.
33. Mecking, H. and U. Kocks, *Kinetics of flow and strain-hardening.* Acta Metallurgica, 1981. **29**(11): p. 1865-1875.
34. Kocks, U., A. Argon, and M. Ashby, *Thermodynamics and kinetics of slip, 1975.* Progress in Materials Science. **19**.
35. Frost, H.J. and M.F. Ashby, *Deformation mechanism maps: the plasticity and creep of metals and ceramics.* 1982.
36. Fisher, J.C., W. Johnston, and R. Thomson, *Dislocations and mechanical properties of crystals*. 1957: Wiley.

37. Bergström, Y., *The Plastic Deformation of Metals: A Dislocation Model and Its Applicability*. 1982: Division of physical metallurgy, Royal Inst. of techn.[Inst. för metallografi, Tekn. högsk.].
38. Estrin, Y., et al., *Thermodynamics, microstructures, and plasticity.* NATO advanced study institute on thermodynamics. Microstructures and plasticity, Kluwer Academic Publishers, France, 2002: p. 217-238.
39. Bergström, Y., *The Plastic Deformation of Metals--a Dislocation Model and Its Applicability.* Rev. Powder Metall. Phys. Ceram., 1983. **2**(2): p. 79-265.
40. Wang, Q., *Microstructural effects on the tensile and fracture behavior of aluminum casting alloys A356/357.* Metallurgical and materials transactions A, 2003. **34**(12): p. 2887-2899.
41. Militzer, M., W. Sun, and J. Jonas, *Modelling the effect of deformation-induced vacancies on segregation and precipitation.* Acta metallurgica et materialia, 1994. **42**(1): p. 133-141.
42. Siwecki, T. and G. Engberg, *Recrystallization controlled rolling of steels.* Thermo-Mechanical Processing in Theory, Modelling & Practice[TMP] exp 2, 1996: p. 121-144.
43. Roters, F., D. Raabe, and G. Gottstein, *Work hardening in heterogeneous alloys—a microstructural approach based on three internal state variables.* Acta materialia, 2000. **48**(17): p. 4181-4189.
44. Fujikawa, S.-i., K.-i. Hirano, and Y. Fukushima, *Diffusion of silicon in aluminum.* Metallurgical Transactions A, 1978. **9**(12): p. 1811-1815.
45. Ogris, E., et al., *On the silicon spheroidization in Al–Si alloys.* Journal of Light Metals, 2002. **2**(4): p. 263-269.
46. Van Gurp, G., *Diffusion-limited Si precipitation in evaporated Al/Si films.* Journal of Applied Physics, 1973. **44**(5): p. 2040-2050.
47. Burton, J., *Vacancy-formation entropy in cubic metals.* Physical Review B, 1972. **5**(8): p. 2948.
48. Xue, Y., et al., *Multistage fatigue modeling of cast A356-T6 and A380-F aluminum alloys.* Metallurgical and Materials Transactions B, 2007. **38**(4): p. 601-606.
49. Mondolfo, L.F., *Aluminum alloys: structure and properties*. 2013: Elsevier.
50. Dieter, G.E. and D.J. Bacon, *Mechanical metallurgy*. Vol. 3. 1986: McGraw-Hill New York.
51. Vollertsen, F. and S. Vogler, *Werkstoffeigenschaften und Mikrostruktur*. 1989: Hanser Muenchen.
52. Banerjee, B. and A. Bhawalkar, *An extended mechanical threshold stress plasticity model: modeling 6061-T6 aluminum alloy.* Journal of Mechanics of Materials and Structures, 2008. **3**(3): p. 391-424.
53. Roswell, A. and A. Nowick, *Decay of Lattice Defects Frozen into an Alloy by Quenching.* Transactions, 1953: p. 1259.
54. Lomer, W., *Vacancies and other point defects in metals and alloys.* Institute of Metals, London, 1958: p. 79.
55. Górecki, T., *Vacancy-Impurity Binding Energy and the Effective Vacancy Formation Energy as Determined from the Solidus Line for Binary Al-Based Alloys.* Berichte der Bunsengesellschaft für physikalische Chemie, 1983. **87**(9): p. 801-803.
56. Ryen, Ø., et al., *Strengthening mechanisms in solid solution aluminum alloys.* Metallurgical and Materials Transactions A, 2006. **37**(6): p. 1999-2006.

57. Babu, B. and L.-E. Lindgren, *Dislocation density based model for plastic deformation and globularization of Ti-6Al-4V.* International Journal of Plasticity, 2013. **50**: p. 94-108.
58. Li, R., et al., *Age-hardening behavior of cast Al–Si base alloy.* Materials Letters, 2004. **58**(15): p. 2096-2101.
59. Rosenbaum, H. and D. Turnbull, *On the precipitation of silicon out of a supersaturated aluminum-silicon solid solution.* Acta Metallurgica, 1958. **6**(10): p. 653-659.
60. Rosenbaum, H. and D. Turnbull, *Metallographic investigation of precipitation of silicon from aluminum.* Acta Metallurgica, 1959. **7**(10): p. 664-674.
61. Zenou, V., et al., *The microscopic mechanism of silicon precipitation in Al/Si system.* Materials Science and Engineering: A, 2006. **435**: p. 556-563.
62. Lasagni, F., et al., *Precipitation kinetics of Si in aluminium alloys.* Materials Science and Engineering: A, 2008. **480**(1): p. 383-391.
63. Zamani, M., S. Seifeddine, and A.E. Jarfors, *High temperature tensile deformation behavior and failure mechanisms of an Al–Si–Cu–Mg cast alloy—The microstructural scale effect.* Materials & Design, 2015. **86**: p. 361-370.